University of Groningen

An upper limit on Gibbs energy dissipation governs cellular metabolism

Niebel, Bastian; Leupold, Simeon; Heinemann, Matthias

IMPORTANT NOTE: You are advised to consult the publisher's version (publisher's PDF) if you wish to cite from it. Please check the document version below.

Document Version
Final author's version (accepted by publisher, after peer review)

[Link to publication in University of Groningen/UMCG research database](#)

An upper limit in Gibbs energy dissipation governs cellular metabolism

Bastian Niebel[$], Simeon Leupold[$] and Matthias Heinemann*

Molecular Systems Biology, Groningen Biomolecular Sciences and Biotechnology Institute,
University of Groningen, Nijenborgh 4, 9747 AG Groningen, The Netherlands

*Corresponding author: m.heinemann@rug.nl (phone +31 50 363 8146)
[$] These authors contributed equally to this work

The principles governing cellular metabolic operation are poorly understood. Because diverse organisms show similar metabolic flux patterns, we hypothesized that a fundamental thermodynamic constraint might shape cellular metabolism. Here, we developed a constraint-based model for *Saccharomyces cerevisiae* with a comprehensive description of biochemical thermodynamics including a Gibbs energy balance. Nonlinear regression analyses of quantitative metabolome and physiology data revealed the existence of an upper rate limit for cellular Gibbs energy dissipation. Applying this limit in flux balance analyses with growth maximization as the objective, our model correctly predicted the physiology and intracellular metabolic fluxes for different glucose uptake rates as well as the maximal growth rate. We found that cells arrange their intracellular metabolic fluxes in such a way that, with increasing glucose uptake rates, they can accomplish optimal growth rates, but stay below the critical rate limit in Gibbs energy dissipation. Once all possibilities for intracellular flux redistribution are exhausted, cells reach their maximal growth rate. This principle also holds for *Escherichia coli* and different carbon sources. Our work proposes that metabolic reaction stoichiometry, a limit in the cellular Gibbs energy dissipation rate, and the objective of growth maximization shape metabolism across organisms and conditions.

A key question in metabolic research is to understand how and why cells organize their metabolism, i.e. their fluxes through the metabolic network, in a particular manner. Such understanding is highly relevant from a fundamental point of view, but also should enable us to devise computational methods for metabolic-flux prediction; an important capability for fundamental biology and biotechnology.

22 The archetype question in this context is why many pro- and eukaryotic cells – also under aerobic

23 conditions – often use an inefficient fermentative metabolism. To this end, numerous explanations were

24 offered, including the economics of enzyme production[1,2], a 'make-accumulate-consume' strategy[3],

25 intracellular crowding[4], limited nutrient transport capacity[5], and adjustments to growth-dependent

26 requirements[6,7]. Recently, the integration of proteome allocation constraints in metabolic models has led

27 to predictions in good agreement with experimental data[8,9]. However, the fact that respiration and aerobic

28 fermentation occur in many organisms, including bacteria[4], fungi[3], mammals[6,7], and plants[10], with

29 fermentation occurring at high glucose uptake rates (GURs) and respiration at low GURs[7,11], prompted us

30 to ask, whether rather a fundamental thermodynamic principle could govern metabolism, on top of which

31 the specific protein allocation constraints have evolved. Specifically, we hypothesized that the rate at

32 which cells, as open and far-from-equilibrium systems[12], can dissipate Gibbs energy to the extracellular

33 environment[13] may be limited and that such a limit, should it exist, may constrain the metabolic fluxes.

34 Here, using a constraint-based thermodynamic model of *Saccharomyces cerevisiae* and nonlinear

35 regression analysis of quantitative metabolome and physiology data, we identified an upper limit for the

36 cellular Gibbs energy dissipation rate. When we used this rate limit in flux balance analyses (FBA) with

37 growth maximization as objective function, we could generate correct predictions of metabolic

38 phenotypes at diverse conditions. As we found the same principle to also hold in *Escherichia coli*, our

39 work suggests that growth maximizing under the constraint of an upper rate limit in Gibbs energy

40 dissipation must have been the general governing principle in shaping metabolism and its regulation.

41 Furthermore, our work provides an important contribution to current predictive metabolic modelling for

42 fundamental biology and biotechnology.

43 **RESULTS**

44 **Development of a combined thermodynamic and stoichiometric model**

45 To test our hypothesis, according to which cellular metabolism is limited by a certain critical rate of

46 Gibbs energy dissipation, we used the yeast *S. cerevisiae* as a model and aimed to estimate cellular Gibbs

47 energy dissipation rates from experimental data using regression analysis (Fig. 1). Specifically, we

48 formulated a combined thermodynamic and stoichiometric metabolic network model, describing cellular

49 metabolic operation through the variables metabolic flux (i.e. reaction rate), *v*, and metabolite

50 concentration, *c*. At the basis of this model is a stoichiometric metabolic network model[14] (Supplementary

51 Method 1.1 and Supplementary Note 1), which describes 241 metabolic processes of primary metabolism

52 (i.e. chemical conversions and metabolite transport, *MET*) and their mitochondrial or cytosolic

53 localization with mass balances for 156 metabolites (Tables 1-5 from Supplementary Data 1) as well as

54 with pH-dependent proton and charge balances (Tables 6 and 7 from Supplementary Data 1). The

55 boundary of the system was defined around the extracellular space and the exchange of matter with the

56 environment was realized through 15 exchange processes (*EXG*) (compare. Fig. 1).

57 To this model, we added a Gibbs energy balance stating that the sum of the Gibbs energy dissipation rates

58 of the individual metabolic processes (i.e. the total cellular rate of Gibbs energy dissipation, g^{diss}) must

59 equal the sum of the rates at which Gibbs energy is exchanged with the environment (Supplementary

60 Method 1.2). We defined the rate of Gibbs energy dissipation of a metabolic process as the product of the

61 metabolic flux of the process and its Gibbs energy. The Gibbs energy of a metabolic process, in turn, was

62 made a function of the substrate and product concentrations, the standard Gibbs energy of the reaction,

63 and/or the Gibbs energy of the metabolite's transmembrane transport[15]. We transformed the standard

64 Gibbs energies of the reaction to the respective compartmental pH values[16] (Supplementary Method 1.3).

65 Finally, for each metabolic process, we added the second law of thermodynamics stating that the Gibbs

66 energy dissipation rate must be negative for a metabolic process carrying flux (Method 1.4). All

67 metabolic processes in the model were considered reversible.

Existence of a limit in the rate of cellular Gibbs energy dissipation

69 To determine cellular Gibbs energy dissipation rates, g^{diss}, at different growth conditions, we analysed

70 experimental data with regression analysis, using the developed model (Supplementary Fig. 1 and

71 Supplementary Method 2.1). Specifically, we used physiological (i.e. growth rates, metabolite uptake and

72 excretion rates) and metabolome data of *S. cerevisiae* obtained from eight different glucose-limited

73 chemostat cultures[17]. In these cultures, metabolic operation ranged from respiration at low GURs to

74 aerobic fermentation with ethanol production at high GURs. As Gibbs energies estimated with the

75 component contribution method[18] contained uncertainties, and Gibbs energies were also not available for

76 all metabolic reactions, we included the available standard Gibbs energies of reaction together with their

77 respective uncertainties as experimental data in the regression.

78 To enforce one common set of standard Gibbs energies of reaction across all experimental conditions

79 with the same thermodynamic reference state (i.e. obeying the first law of thermodynamics, which we

80 enforced by applying the loop law[19,20]), we performed one large regression across all conditions. In this

81 large-scale multi-step nonlinear regression, we estimated for each condition its condition-dependent

82 variables (i.e. fluxes, metabolite concentrations), and for all conditions together, a set of condition-

83 independent standard Gibbs energies of reaction with minimal distance to the experimental data.

84 To prevent overfitting, we employed a parametric bootstrap approach (Supplementary Fig. 2a). The

85 regression and a subsequent variability analysis of the solution space provided us with physiological

86 ranges for the intracellular metabolite concentration and for the Gibbs energies of reaction (i.e. the lowest

87   and highest possible values across all experimental conditions reflecting the physiological bounds of

88   metabolic operation), which we used to refine the scope of the model (Supplementary Method 2.2 and

89   Tables 8 and 9 from Supplementary Data 1).

90   First, we found that the model with its thermodynamic and stoichiometric constraints could excellently be

91   fitted to all data sets (Supplementary Fig. 2b-d), demonstrating that the developed model is able to

92   describe the broad range of underlying metabolic operations, ranging from fully respiratory to

93   fermentative conditions. Second, examining the cellular Gibbs energy dissipation rates, g^{diss}, determined

94   for the different experimental conditions, we found that g^{diss} first linearly increased with increasing

95   growth rate μ, and then plateaued at μ's above 0.3 h^{-1} (Fig. 2). The existence of a plateau above a certain

96   μ suggested – in line with our hypothesis – that there could be an upper rate limit, g^{diss}_{lim}, at which cells

97   can dissipate Gibbs energy; here corresponding to -3.7 kJ gCDW^{-1} h^{-1}. Because the growth rate, at which

98   this limit is reached, coincided with the onset of ethanol excretion, we speculated that this limit might

99   cause the switch to fermentation at high GURs.

Accurate predictions of metabolic phenotypes

101   To test whether such an upper limit in the Gibbs energy dissipation rate might govern metabolic

102   operation, i.e. might be responsible for the different flux distributions at different GURs, we resorted to

103   flux balance analysis, which computes metabolic flux distributions on the basis of a stoichiometric

104   metabolic network model and mathematical optimization using an evolutionary optimization criterium[14].

105   Specifically, we used the objective of growth maximization (i.e. identifying the flux distribution that

106   generates the maximal amount of biomass from the available nutrients) to simulate the combined

107   thermodynamic and stoichiometric model, which we now additionally constrained by the hypothesized

108   upper limit in the Gibbs energy dissipation rate, g^{diss}_{lim} (Supplementary Method 2.2). To solve this non-

109   convex bilinear optimization problem, we transferred it into a mixed integer nonlinear program, which we

110   then solved using a branch-and-cut global optimization algorithm[21] (Supplementary Methods 1.5, 1.6 and

111   2.3).

112   While the objective of growth maximization alone could not predict flux distributions across experimental

113   conditions[22], using it in combination with the identified upper limit in g^{diss} we could correctly predict

114   physiologies as observed in glucose-limited chemostat cultures and in glucose batch cultures, solely using

115   the respective glucose uptake rates as input. For instance, growth rates were correctly predicted (Fig. 3a),

116   and a respiratory metabolism at low GURs (< 3 mmol gCDW^{-1} h^{-1}, Fig. 3b-d) and aerobic fermentation

117   with lowered oxygen uptake rates at GURs > 3 mmol gCDW^{-1} h^{-1} (Fig. 3b and c). At a GUR of 22 mmol

118   gCDW^{-1} h^{-1}, we predicted a maximal growth rate, followed by a decrease in the growth rate and glycerol

119   production at further increased GURs, notably while still maximizing the growth rate in the optimization.

120   FBA simulations without a limit in g^{diss} predicted a respiratory metabolism for all GURs, and no maximal

121   growth rate (compare dotted lines in Fig. 3a-d) and FBA simulations with other frequently-used

122   objectives ('minimal sum of absolute fluxes', 'maximal ATP yield', 'maximal ATP yield per flux sum',

123   'maximal biomass per biomass') and the g^{diss}_{lim}-constraint were unable to correctly predict the

124   physiologies (compare dashed lines in Fig. 3a-d and Supplementary Fig. 6). Together with exhaustive

125   sensitivity analyses with regards to various model parameters, e.g. lower and upper bounds of the

126   intracellular metabolite concentrations, and Gibbs energies of reaction (Supplementary Fig. 3-5), this

127   shows, that the excellent predictions obtained with growth maximization as objective and the constrained

128   cellular Gibbs energy dissipation rate are not a trivial result of the earlier regression, nor are enforced by

129   isolated elements of our model.

130   To further examine the predictions obtained with the model constrained by the rate limit in Gibbs energy

131   dissipation, we compared intracellular flux predictions with results from ^{13}C-based metabolic flux

132   analysis (^{13}C-MFA). Here, we found that our predictions are in excellent agreement with fluxes

133   determined with ^{13}C-MFA, as evident from metabolic reactions located at key branch points in central

134   metabolism (Fig. 4a-d and Supplementary Fig. 7). We found the expected flux reorganization patterns; for

135   instance, redirection of flux from the pentose-phosphate pathway to glycolysis with increasing GUR (Fig.

136   4a and b).

137   The fact that we could correctly predict extracellular physiologies including the maximal growth rate, as

138   well as the experimentally observed reorganization pattern of intracellular metabolic fluxes with

139   increasing GURs suggests that the objective of growth maximization under the constraint of an upper

140   limit in the Gibbs energy dissipation rate could have been the governing principle in the evolution of

141   metabolism and its regulation, at least in yeast.

142   **Identified principle also applies to *E. coli***

143   Because we conjectured that the two elements of this principle, i.e. growth maximization and the upper

144   limit in the Gibbs energy dissipation rate might be of universal nature, next, using *E. coli* as model, we

145   investigated whether this principle also applies to prokaryotes. Following the same workflow as outlined

146   for *S. cerevisiae,* we formulated a combined thermodynamic and stoichiometric metabolic model; this

147   time in genome-scale, encompassing 626 unique metabolites involved in 1062 metabolic processes[29]

148   (Supplementary Methods 1.1-1.5, Supplementary Note 2 and Supplementary Data 2). Using this model

149   and nonlinear regression (Supplementary Methods 3.1 and 3.2) with data from glucose-limited chemostat

150   cultures[30], we found, similar to yeast, that the cellular Gibbs energy dissipation rate, g^{diss}, first linearly

151   increased with increasing GURs and then reached a plateau (at -4.9 kJ gCDW^{-1} h^{-1}), at conditions where

152   acetate is excreted (Supplementary Fig. 9 and 10). When we performed FBA simulations with growth

153 maximization as objective, and the identified upper rate limit in Gibbs energy dissipation, g^{diss}_{lim}, as
154 constraint (Supplementary Methods 3.3 and 3.4), we again correctly predicted the metabolic shift from
155 respiration to fermentation with increasing GURs, as well as the maximal growth rate (Fig. 5a). Notably,
156 we found this flux reorganization pattern to be reflected in measured changes in protein abundances
157 (Supplementary Fig. 11).

158 Next, we used this model to perform FBA simulations with different nutrients, where we allowed for
159 unlimited substrate uptake. Specifically, we simulated growth in unlimited batch cultures on eight
160 different carbon sources (acetate, fructose, galactose, gluconate, glucose, glycerol, pyruvate and
161 succinate), on simultaneously present glucose and succinate, and on either glucose or glycerol
162 supplemented with all proteinogenic amino acids; notably all conditions that were not used in the
163 regression. Here, we found that our model could across the board predict the maximal growth rates, as
164 well as uptake and excretion rates (Fig. 5b and Supplementary Fig. 12). Remarkably, this was even true
165 for the cases where we simulated complex media with the possibility of unlimited uptake of all
166 proteinogenic amino acids. The same model, not constrained by the upper rate limit in Gibbs energy
167 dissipation, is not able to predict maximal growth rates (as maximization of growth would lead to an
168 infinite substrate uptake and thus to infinite growth), and failed to predict the fermentative phenotypes
169 (Supplementary Fig. 13). A comparison of the FBA predicted intracellular fluxes with ^{13}C-based MFA-
170 inferred flux distributions showed good agreement (Supplementary Fig. 14).

171 As our model connects fluxes and metabolite levels through the Gibbs energies of reaction, we next asked
172 whether the metabolic rearrangements, necessary with increasing GURs, would require metabolite levels
173 to follow certain trends. Indeed, for 36 metabolites we found a correlation (Spearman correlation
174 coefficient >0.6) between their concentrations and GUR. Of these 36 metabolites, experimental data as a
175 function of GUR were available for coenzyme A, ribose 5-phosphate and α-ketoglutarate. The profiles of
176 these metabolites remarkably well matched with the predicted profiles (Fig. 5c). Notably, α-ketoglutarate
177 has been identified as an important metabolic regulator molecule[31]. Our analysis here suggests that the
178 concentration of this metabolite is constrained in a GUR-dependent manner by thermodynamics, and thus
179 having made it an ideal candidate as regulatory metabolite.

180 With these *E. coli* predictions agreeing well with respective experimental data, extending even to the
181 predictions of some metabolite concentrations, this suggests that growth maximization under the
182 constraint of a limited cellular Gibbs energy dissipation rate as metabolism-governing principle also
183 applies to *E. coli* and carbon sources other than glucose, including complex media. This provides strong
184 evidence for this principle to universally shaping cellular metabolism across organisms. Further, as the *E.*

185 *coli* model was a genome-scale model, this shows that the concept can also be implemented and applied
186 on the genome-scale.

Maximal growth under the rate limit in Gibbs energy dissipation

188 Finally, we aimed to understand how the upper limit in Gibbs energy dissipation rate, g^{diss}_{lim}, governs
189 metabolism. Therefore, we went back to yeast and the respective flux balance analyses simulations, from
190 which we determined the Gibbs energy dissipation rate of each metabolic process, g, at different GURs.
191 From these process- and GUR-specific dissipation rates, we identified seven clusters of metabolic
192 processes that showed similar Gibbs energy dissipation trends with increasing GURs (Fig. 6a and
193 Supplementary Fig. 15). Below GURs of 3 mmol $gCDW^{-1}$ h^{-1}, we found that the processes related to
194 respiration (respiration and energy metabolism clusters in Fig. 6a) contributed 45% to the total cellular
195 Gibbs energy dissipation rate, which - in absolute terms - is still low at this point. After, with increasing
196 GUR, g^{diss}_{lim} is reached, cells redirected metabolic fluxes from dissipation-intense pathways to less
197 dissipation-intense pathways, i.e. to fermentative processes (pyruvate decarboxylase and pyruvate kinase
198 clusters in Fig. 6a), which produced about 40% of the g^{diss} at GURs above 20 mmol $gCDW^{-1}$ h^{-1}.

199 Such flux redirection not only occurred between respiration and fermentation, but also between other
200 processes as indicated by the changes in the directionality patterns (Supplementary Fig. 17). Thus, the
201 flux redirection, which occurs at increasing GURs, allows cells to achieve higher growth rates, while
202 staying below g^{diss}_{lim}. Such flux redirection results in usage of pathways with lower carbon efficiencies
203 and thus lower biomass yields (Fig. 6b). Once all possibilities for flux redirections are exhausted, upon a
204 further enforced increase in the nutrient uptake, cells – in order to stay below the Gibbs energy dissipation
205 rate limit – need to reduce their growth rate and to excrete other by-products (for instance, glycerol),
206 which defines the maximal growth rate (compare Fig. 2).

DISCUSSION

208 Our finding answers central questions in metabolic research, e.g. what shapes metabolic fluxes, what
209 limits growth rate, and what causes cells to change the way they operate their metabolism, as exemplified
210 by the paradigm switch from respiration to aerobic fermentation. Although we cannot exclude the
211 existence of a third correlated factor explaining our results, our work proposes growth maximization
212 under the constraint of an upper limit in the cellular Gibbs energy dissipation rate as the basic principle
213 underlying metabolism; also offering an explanation for the empirical description of Pareto-optimality in
214 metabolism[40] (Supplementary Fig. 18). The limit in cellular Gibbs energy dissipation rate leads to a
215 redirection of metabolic fluxes (for instance, from respiration to fermentation) as substrate uptake rates
216 increase, and cells try to maximize growth.

217   While traditionally only having been formulated for isolated systems close to equilibrium[12], here we used

218   the second law of thermodynamics for cells as open, out-of-equilibrium systems, as applied previously for

219   cellular metabolism[13,41–47]. Following Erwin Schrödinger's notion that *"the essential thing in metabolism*

220   *is that the organism succeeds in freeing itself from all the entropy it cannot help producing while alive"*[48],

221   our work suggests that there exists an upper rate limit at which cells can do so.

222   The identified upper rate limit in cellular Gibbs energy dissipation suggests that higher rates of Gibbs

223   energy dissipation cannot be sustained, because this presumably has detrimental consequences for the

224   functioning of cells. What could such consequences be? If the dissipated Gibbs energy is dissipated as

225   heat, then the identified limit could be understood as a limit in heat transfer. Although it was suggested

226   that mitochondria (notably a compartment where at certain conditions we predicted >50 % of the total

227   cellular Gibbs energy dissipation, compare Fig. 6) could have an elevated temperature[49,50], theoretical

228   considerations argue against a significant and detrimental temperature increase inside individual cells[51].

229   On the other hand, during their catalytic cycle, enzymes are set in motion and Gibbs energy is therefore

230   translated into work[52–55]. In fact, active metabolism has been found to increase cytoplasmic diffusion rates

231   above the ones expected from thermal motion alone[56–58]. In turn, cytoplasmic motion was shown to

232   negatively affect biomolecular functions, such as kinetic proofreading and gene regulation[59,60]. It is thus

233   possible that the upper limit in the rate of cellular Gibbs energy dissipation reflects the limit of critical

234   non-thermal motion inside the cell, beyond which biomolecular function would be compromised.

235   To maximize growth rate and at the same time avoid exceeding the critical Gibbs energy dissipation rate,

236   cells need to have evolved respective sensing mechanisms and means to control metabolic fluxes by

237   adjusting enzyme abundance and kinetics. If indeed cytoplasmic motion reflects the cellular Gibbs energy

238   dissipation rate, then this could directly lead to differential regulation of gene expression. Alternatively,

239   the recently uncovered cellular capability for metabolic flux sensing and flux-dependent regulation[11,61]

240   could have evolved in a manner to ultimately avoid detrimental Gibbs energy dissipation rates.

241   Our approach of a limit in the cellular Gibbs energy dissipation rate is structurally similar to recent

242   approaches using protein allocations constraints[8,9], with a weighted sum of fluxes being the limiting

243   element in both. In the protein allocation approaches, metabolic fluxes are weighted e.g. by the molecular

244   mass and the catalytic efficiency of the respective enzymes[9]. In contrast to these static weights, in our

245   approach, the weighting is provided by the Gibbs energies of reaction, which - being a function of flexible

246   metabolite concentrations - can vary to some extent. We argue that the similarity is not only of technical

247   nature, but likely has a biological or physical reason: To harness the energy, which is released during

248   catabolism, cells need to partition their metabolism into reaction steps that release Gibbs energy amounts

249   that can be stored, e.g. as ATP. Thus, an overall larger change in Gibbs energy in a pathway (e.g. as in

250 respiration compared to fermentation) requires a higher number of reaction steps, and thus a larger
251 amount of enzyme.

252 Our work presents a fundamental understanding of metabolism, i.e. that the operation of cellular
253 metabolism is constrained by a limit in the cellular Gibbs energy dissipation rate. This limit is likely a
254 universal, physical constraint on metabolism and could also explain the Warburg effect in cancer cells.
255 Future work will need to show how the Gibbs energy dissipation rate limits biomolecular function, and
256 how it could have shaped the evolution of enzyme expression and kinetics. Moreover, our concept for
257 metabolic flux prediction, although computationally demanding, can offer an advantage over current
258 FBA-based methods as it does not require assumptions on reaction directionalities, and does not require
259 any organism-specific hard-to-obtain information on e.g. protein abundances and catalytic efficiencies[62].
260 Thus, with this work, we not only present a fundamental understanding of metabolism, but also provide
261 an important contribution to predictive metabolic modelling.

270 **Author Contributions**
271 BN, SL and MH designed the study. BN and MH developed the concept. BN developed and implemented
272 the model for *S. cerevisiae*. SL developed and implemented the model for *E. coli*. BN and SL carried out
273 the simulations, analysed the data, and made the figures. BN, SL and MH wrote the manuscript.

274 **Data availability**
275 The data that support the plots within this paper and other findings of this study are available from the
276 corresponding author upon reasonable request. The code is available from the corresponding author upon
277 request and the code to perform the flux balance analyses is deposited on GitHub (DOI:
278 10.5281/zenodo.1401220).

279 **Competing interests**
280 The authors declare no competing interests.

METHODS

Formulation of the combined thermodynamic and stoichiometric model

The combined thermodynamic and stoichiometric network model rests on steady-state mass balances for the metabolites i,

$$\sum_{j \in MET} S_{ij} v_j = v_{i \in EXG} \quad \forall i \quad , \text{Eq. 1}$$

where S_{ij} are the stoichiometric coefficients of the metabolic ($j \in MET$) and exchange ($i \in EXG$) processes; $v_{j \in MET}$ are the rates of metabolic processes, i.e. chemical conversions and/or metabolite transport; and $v_{i \in EXG}$ are the rates of exchange processes, which describe the transfer of metabolites across the system boundary. In this stoichiometric network model, we included for each intra-cellular compartment steady-state pH-dependent proton and charge balances, enforcing that the metabolic fluxes are such that the pH in the respective compartments and the membrane potentials across the membranes are kept constant (Supplementary Method 1.1).

Next to the mass, proton and charge balances, we introduced a Gibbs energy balance, which states that the cellular Gibbs energy dissipation rate, g^{diss}, equals the sum of Gibbs energy exchange rates, $g_{i \in EXG}$, and the sum of Gibbs energy dissipation rates, $g_{j \in MET}$,

$$g^{diss} = \sum_{i \in EXG} g_i = \sum_{j \in MET} g_j \quad . \text{Eq. 2}$$

The Gibbs energy exchange rates are defined as,

$$g_i = \Delta_f G'_i v_i \quad \forall i \in EXG \quad , \text{Eq. 3}$$

where $\Delta_f G'_{i \in EXG}$ are the Gibbs energies of formation of the metabolites transferred across the system boundary. The Gibbs energy dissipation rates are defined as,

$$g_j = \Delta_r G'_j v_j \quad \forall j \in MET \quad , \text{Eq. 4}$$

where $\Delta_r G'_{j \in MET}$ are the Gibbs energies of reaction of the cellular metabolic processes.

The Gibbs energies of reaction of the metabolic processes, $\Delta_r G'_{j \in MET}$, are due to chemical conversions and/or metabolite transport according to,

$$\Delta_r G'_j = \Delta_r G'^o_j + \Delta_r G'^t_j + RT \sum_{i \notin h^+} S_{ij} \ln c_i \quad \forall j \in MET \quad , \text{Eq. 5}$$

where $\Delta_r G'^o_{j \in MET}$ are the standard Gibbs energies of the chemical conversions, $\Delta_r G'^t_{j \in MET}$ the Gibbs energies of the metabolite transports, $\ln c_i$ the natural logarithm of the concentration c_i of the metabolite i, T the temperature and R the universal gas constant.

To define the Gibbs energy exchange rates, we used Gibbs energies of formations, $\Delta_f G'_{i \in EXG}$, of the respective metabolites $i \in EXG$ that are transferred across the system boundary,

$$\Delta_f G'_i = \Delta_f G'^o_i + RT \ln c_i \quad i \in EXG \quad , \text{Eq. 6}$$

where $\Delta_f G'^o_{i \in EXG}$ are the standard Gibbs energies of formation of the metabolites $i \in EXG$.

11

313   All standard Gibbs energies were estimated using the component-contribution method[18] and transformed[16] (indicated

314   by the apostrophe) to the pH values in the respective compartment. Further, we used the extended Debye-Hückel

315   equation to take into account the effect of electrolyte solution on charged metabolites[16] (Supplementary Methods 1.2

316   and 1.3).

317   The directionalities of the fluxes through the metabolic processes $j \in MET$ were in principle assumed to be

318   reversible but need to obey the second law of thermodynamics, according to,

319
$$g_j < 0 \quad \forall \left(j \in MET \wedge v_j \neq 0 \right) \text{, Eq. 7}$$

320   where the Gibbs energy dissipation rate, $g_{j \in MET}$, has to be smaller than zero, in case there is flux through this

321   metabolic process (Supplementary Method 1.4).

322   Combining the relevant equations mentioned above, we formulated the combined thermodynamic and stoichiometric

323   model, $M(v, \ln c) \leq 0$, as a set of equalities and inequalities of the variables v, i.e. the rates of the metabolic processes

324    $j \in MET$ and the exchange processes $i \in EXG$ and $\ln c$, i.e. the natural logarithm of the concentrations of the

325   metabolites i:

326
$$\{M(v, \ln c) \leq 0\} \Rightarrow \begin{cases} \sum_{j \in MET} S_{ij} v_j = v_{i \in EXG} & \forall i \\ g^{\text{diss}} = \sum_{i \in EXG} g_i \\ g^{\text{diss}} = \sum_{j \in MET} g_j \\ g_j = \Delta_r G'_j v_j & \forall j \in MET \\ g_i = \Delta_f G'_i v_i & \forall i \in EXG \\ \Delta_r G'_j = \Delta_r G'^o_j + \Delta_r G'^t_j + RT \sum_{i \neq h^+} S_{ij} \ln c_i & \forall j \in MET \\ \Delta_f G'_i = \Delta_f G'^o_i + RT \ln c_i & i \in EXG \\ g_j < 0 & \forall \left(j \in MET \wedge v_j \neq 0 \right) \end{cases} \text{. Eq. 8}$$

327   Before performing mathematical optimizations with this non-linear and non-convex model, we applied two

328   strategies to reduce the model size, without reducing the model's degrees of freedom. First, we defined the scope of

329   the predictions in terms of allowed exchange processes and removed all reactions from the model that could never

330   carry any metabolic flux under the specified conditions. Second, we identified reactions, which are fully coupled

331   (i.e. carry proportionally always the same flux) as done in Ref. [63] and reformulated the model, $M(v, \ln c) \leq 0$, by

332   replacing the reaction fluxes v with the flux through the group of coupled reactions, v^{grp}. Note that the reduced

333   model, $M^{\text{grp}}(v, \ln c) \leq 0$, strictly still only depends on the fluxes v and metabolite concentrations $\ln c$ and that while

334   the mass balances and Gibbs energy balance are formulated using the flux through the reaction groups v^{grp}, the

335   second law of thermodynamics is still formulated for every metabolic process individually to not lose any

336   directionality constraints.

337   The reduced model together with a set of bounds, $B(v, \ln c) \leq 0$, on the variables v and $\ln c$, define the solution space

338   Ω. Ω contains the space of mass-, proton- and charge-balanced and thermodynamically-feasible steady-state

339   solutions, in terms of rates v and metabolite concentrations ln c. The set of bounds, $B(v, \ln c) \leq 0$, consist of

340   constraints on the rates of the extracellular exchange processes, e.g. the uptake rate of a carbon source, the

341   physiological ranges of the intracellular metabolite concentrations, ln c, and Gibbs energies of reactions, $\Delta_r G'$, or an

342   upper limit in the cellular Gibbs energy dissipation rate, g^{diss}. We analyzed the solution space of the metabolic

343   network model, Ω, using mathematical optimization, where we formulated different optimization problems, e.g.

344   regression-, flux balance- and variability analyses (Supplementary Method 1.5).

345 **Implementation**

346   Because Ω is non-convex and non-linear, the optimization problems can contain multiple local optima. In order to

347   efficiently solve these problems, we first determined an approximate solution by solving a linear relaxation of the

348   optimization problem with the mixed integer programming solver CPLEX 12 (IBM ILOG, Armonk, USA). Then,

349   we used this approximate solution as starting point for the solution of the optimization problem with the global

350   optimization solver ANTIGONE 1.0[21] or the local solver CONOPT3[64].

351   Generally, we implemented all optimization problems in the mathematical programming system GAMS (GAMS

352   Development Corporation. General Algebraic Modeling System (GAMS) Release 24.2.2. Washington, DC, USA).

353   The optimization problems were solved on computational clusters, where we used for the model development and

354   testing a small test cluster, which consisted of 30 cores. For the large-scale studies, where we solved > 100000

355   optimization problems, we set up a cluster in Amazon's Elastic Compute Cloud, which consisted of 1248 cores, or

356   used a managed HPC cluster, which consisted of 5640 cores. Solving these optimization problems typically took

357   between 30 minutes and 14 hours (Supplementary Method 1.6).

358 **Regression analysis**

359   We estimated the cellular rates of Gibbs energy dissipation, g^{diss}, and a thermodynamic consistent set of standard

360   Gibbs energies of reactions, $\Delta_r G'^o$, from experimental data and the reduced model, $M^{grp}(v, \ln c) \leq 0$. The

361   experimental data consisted of (i) measured extracellular physiological rates and (ii) intracellular metabolite

362   concentrations (only in case of *S. cerevisiae*), both determined for glucose-limited chemostat cultures at different

363   dilution rates, and (iii) standard Gibbs energies of reactions, determined from the component contribution method[18].

364   We formulated a non-linear regression analysis that we regularized by the Lasso method[65]. This regularization—

365   done to prevent over fitting the data—included a regularization parameter α, which was determined by model

366   selection. The regression consisted of two steps: (i) determining the minimal training error as a function of α and (ii)

367   determining the goodness of fit using the reduced chi square $\chi^2_{red,\alpha}$ as a function of α. The model selection was

368   performed by repeating these two steps for different α and selecting the α with a reduced chi square $\chi^2_{red,\alpha}$ of 1,

369   which means that the model and the data fit each other (Supplementary Methods 2.1 and 3.1).

370   Next, we determined physiological bounds for the Gibbs energies, $\Delta_r G'_{j \in MET}$, of the metabolic processes $j \in MET$

371   and for the metabolite concentrations, c_i. These physiological bounds (lower *lo*, and upper *up*) are required in our

372   strategy to solve the flux balance analyses optimizations to formulate the linear relaxation and were defined by the

373　infimum and supremum, i.e. the smallest and greatest possible values of c and $\Delta_r G'$ across all experimental

374　conditions of the data sets as determined by variability analysis (Supplementary Methods 2.2 and 3.2).

375　**Flux balance analysis with the combined thermodynamic and stoichiometric model**

376　For different growth conditions, i.e. glucose uptake rates or carbon sources, we predicted metabolic fluxes using the

377　reduced model, $M^{grp}(v, \ln c) \leq 0$, and flux balance analysis. Therefore, we defined the solution spaces of the flux

378　balance analysis, Ω^{FBA}: The metabolite concentrations, $\ln c$, and the Gibbs energies of reaction, $\Delta_r G'$, were

379　constrained by the in the regression identified physiological bounds, and the standard Gibbs energies of reactions,

380　$\Delta_r G'^o$, were set to the identified thermodynamic consistent set. Furthermore, the cellular Gibbs energy dissipation

381　rate, g^{diss}, was constrained by its identified upper limit g^{diss}_{lim} and the rates of exchange processes were constrained

382　by the growth condition, such that any quantity of oxygen, phosphate, ammonium, water, protons, sulfate, etc.

383　(resembling of what was available in the growth medium) could be taken up, and all other compounds could be

384　excreted.

385　Then, we used flux balance analysis[14], where we maximized the growth rate, μ, in the solution space Ω^{FBA},

386
$$\mu^* = \max\left\{v_{BMSYN} : (v, \ln c) \in \Omega^{FBA}\right\} \quad , \text{Eq. 9}$$

387　where μ^* is the optimal growth rate at a specific condition, and BMSYN is the biomass synthesis reaction

388　(Supplementary Methods 2.3 and 3.3).

389　We then characterized the solution space $\Omega^{FBA}_{\mu^*}$ for optimal growth rates, using flux variability analysis, and, as

390　done earlier[14,40,66], using Markov Chain Monte Carlo (MCMC) sampling (Supplementary Methods 2.4 and 3.4).

391　**References**

392　1.　Molenaar, D., Van Berlo, R., De Ridder, D. & Teusink, B. Shifts in growth strategies reflect

393　　　tradeoffs in cellular economics. *Mol. Syst. Biol.* **5,** (2009).

394　2.　Basan, M. *et al.* Overflow metabolism in Escherichia coli results from efficient proteome

395　　　allocation. *Nature* **528,** 99–104 (2015).

396　3.　Rozpędowska, E. *et al.* Parallel evolution of the make–accumulate–consume strategy in

397　　　Saccharomyces and Dekkera yeasts. *Nat. Commun.* **2,** 302 (2011).

398　4.　Beg, Q. K. *et al.* Intracellular crowding defines the mode and sequence of substrate uptake by

399　　　Escherichia coli and constrains its metabolic activity. *Proc. Natl. Acad. Sci. U. S. A.* **104,** 12663–8

400　　　(2007).

401　5.　Zhuang, K., Vemuri, G. N. & Mahadevan, R. Economics of membrane occupancy and respiro-

402　　　fermentation. *Mol. Syst. Biol.* **7,** 500–500 (2014).

403   6.   Koppenol, W. H., Bounds, P. L. & Dang, C. V. Otto Warburg's contributions to current concepts
404   of cancer metabolism. *Nat. Rev. Cancer* **11,** 325–337 (2011).

405   7.   Vander Heiden, M. G., Cantley, L. C. & Thompson, C. B. Understanding the Warburg Effect: The
406   Metabolic Requirements of Cell Proliferation. *Science (80-.).* **324,** 1029–1033 (2009).

407   8.   Mori, M., Hwa, T., Martin, O. C., De Martino, A. & Marinari, E. Constrained Allocation Flux
408   Balance Analysis. *PLOS Comput. Biol.* **12,** e1004913 (2016).

409   9.   Sánchez, B. J. *et al.* Improving the phenotype predictions of a yeast genome-scale metabolic
410   model by incorporating enzymatic constraints. *Mol. Syst. Biol.* **13,** 935 (2017).

411   10.   Zabalza, A. *et al.* Regulation of respiration and fermentation to control the plant internal oxygen
412   concentration. *Plant Physiol.* **149,** 1087–98 (2009).

413   11.   Huberts, D. H. E. W., Niebel, B. & Heinemann, M. A flux-sensing mechanism could regulate the
414   switch between respiration and fermentation. *FEMS Yeast Res.* **12,** 118–128 (2012).

415   12.   von Bertalanffy, L. The theory of open systems in physics and biology. *Science* **111,** 23–9 (1950).

416   13.   von Stockar, U. Biothermodynamics of live cells: a tool for biotechnology and biochemical
417   engineering. *J. Non-Equilibrium Thermodyn.* **35,** 415–475 (2010).

418   14.   Lewis, N. E., Nagarajan, H. & Palsson, B. O. Constraining the metabolic genotype–phenotype
419   relationship using a phylogeny of in silico methods. *Nat. Rev. Microbiol.* **10,** 291–305 (2012).

420   15.   Jol, S. J., Kümmel, A., Hatzimanikatis, V., Beard, D. A. & Heinemann, M. Thermodynamic
421   calculations for biochemical transport and reaction processes in metabolic networks. *Biophys. J.*
422   **99,** 3139–44 (2010).

423   16.   Alberty, R. a *et al.* Recommendations for terminology and databases for biochemical
424   thermodynamics. *Biophys. Chem.* **155,** 89–103 (2011).

425   17.   Canelas, A. B., Ras, C., ten Pierick, A., van Gulik, W. M. & Heijnen, J. J. An in vivo data-driven
426   framework for classification and quantification of enzyme kinetics and determination of apparent
427   thermodynamic data. *Metab. Eng.* **13,** 294–306 (2011).

428   18.   Noor, E., Haraldsdóttir, H. S., Milo, R. & Fleming, R. M. T. Consistent estimation of Gibbs

429   energy using component contributions. *PLoS Comput. Biol.* **9,** e1003098 (2013).

430   19.   Beard, D. a, Liang, S. & Qian, H. Energy balance for analysis of complex metabolic networks.

431   *Biophys. J.* **83,** 79–86 (2002).

432   20.   Price, N. D., Famili, I., Beard, D. A. & Palsson, B. Ø. Extreme pathways and Kirchhoff's second

433   law. *Biophys. J.* **83,** 2879–82 (2002).

434   21.   Misener, R. & Floudas, C. A. ANTIGONE: Algorithms for coNTinuous / Integer Global

435   Optimization of Nonlinear Equations. *J Glob Optim* **59,** 503–526 (2014).

436   22.   Schuetz, R., Kuepfer, L. & Sauer, U. Systematic evaluation of objective functions for predicting

437   intracellular fluxes in Escherichia coli. *Mol. Syst. Biol.* **3,** 119 (2007).

438   23.   van Hoek, P. *et al.* Effects of pyruvate decarboxylase overproduction on flux distribution at the

439   pyruvate branch point in Saccharomyces cerevisiae. *Appl. Environ. Microbiol.* **64,** 2133–40

440   (1998).

441   24.   Kümmel, A. *et al.* Differential glucose repression in common yeast strains in response to HXK2

442   deletion. *FEMS Yeast Res.* **10,** 322–332 (2010).

443   25.   van Winden, W. *et al.* Metabolic-flux analysis of CEN.PK113-7D based on mass isotopomer

444   measurements of C-labeled primary metabolites. *FEMS Yeast Res.* **5,** 559–568 (2005).

445   26.   Fendt, S.-M. & Sauer, U. Transcriptional regulation of respiration in yeast metabolizing differently

446   repressive carbon substrates. *BMC Syst. Biol.* **4,** 12 (2010).

447   27.   Gombert, A. K., Moreira dos Santos, M., Christensen, B. & Nielsen, J. Network Identification and

448   Flux Quantification in the Central Metabolism of Saccharomyces cerevisiae under Different

449   Conditions of Glucose Repression. *J. Bacteriol.* **183,** 1441–1451 (2001).

450   28.   Frick, O. & Wittmann, C. Characterization of the metabolic shift between oxidative and

451   fermentative growth in Saccharomyces cerevisiae by comparative 13 C flux analysis. *Microb. Cell*

452   *Fact.* **4,** 30 (2005).

453   29.   Reed, J. L., Vo, T. D., Schilling, C. H. & Palsson, B. O. An expanded genome-scale model of

454   Escherichia coli K-12 (iJR904 GSM/GPR). *Genome Biol.* **4,** R54 (2003).

455   30.   Vemuri, G. N., Altman, E., Sangurdekar, D. P., Khodursky, A. B. & Eiteman, M. A. Overflow

456   metabolism in Escherichia coli during steady-state growth: transcriptional regulation and effect of

457   the redox ratio. *Appl. Environ. Microbiol.* **72,** 3653–61 (2006).

458   31.   You, C. *et al.* Coordination of bacterial proteome with metabolism by cyclic AMP signalling.

459   *Nature* **500,** 301–306 (2013).

460   32.   Perrenoud, A. & Sauer, U. Impact of Global Transcriptional Regulation by ArcA, ArcB, Cra, Crp,

461   Cya, Fnr, and Mlc on Glucose Catabolism in Escherichia coli. *J. Bacteriol.* **187,** 3171–3179

462   (2005).

463   33.   Valgepea, K. *et al.* Systems biology approach reveals that overflow metabolism of acetate in

464   Escherichia coli is triggered by carbon catabolite repression of acetyl-CoA synthetase. *BMC Syst.*

465   *Biol.* **4,** 166 (2010).

466   34.   Nanchen, A., Schicker, A. & Sauer, U. Nonlinear dependency of intracellular fluxes on growth

467   rate in miniaturized continuous cultures of Escherichia coli. *Appl. Environ. Microbiol.* **72,** 1164–

468   72 (2006).

469   35.   Peebo, K. *et al.* Proteome reallocation in Escherichia coli with increasing specific growth rate.

470   *Mol. BioSyst. Mol. BioSyst* **11,** 1184–1193 (1184).

471   36.   Gerosa, L. *et al.* Pseudo-transition Analysis Identifies the Key Regulators of Dynamic Metabolic

472   Adaptations from Steady-State Data. *Cell Syst.* **1,** 270–282 (2015).

473   37.   Gerosa, L. *et al.* Pseudo-transition Analysis Identifies the Key Regulators of Dynamic Metabolic

474   Adaptations from Steady-State Data. *Cell Syst.* (2015). doi:10.1016/j.cels.2015.09.008

475   38.   Schmidt, A. *et al.* The quantitative and condition-dependent Escherichia coli proteome. *Nat.*

476   *Biotechnol.* **34,** 104–110 (2015).

477   39.   Scott, M. *et al.* Emergence of robust growth laws from optimal regulation of ribosome synthesis.

478   *Mol. Syst. Biol.* **10,** 747 (2014).

479   40.   Schuetz, R., Zamboni, N., Zampieri, M., Heinemann, M. & Sauer, U. Multidimensional

Optimality of Microbial Metabolism. *Science (80-.).* **336,** 601–604 (2012).

41. Beard, D. A., Liang, S. & Qian, H. Energy Balance for Analysis of Complex Metabolic Networks. *Biophys. J.* **83,** 79–86 (2002).

42. Kümmel, A., Panke, S. & Heinemann, M. Putative regulatory sites unraveled by network-embedded thermodynamic analysis of metabolome data. *Mol. Syst. Biol.* **2,** 2006.0034 (2006).

43. Henry, C. S., Broadbelt, L. J. & Hatzimanikatis, V. Thermodynamics-Based Metabolic Flux Analysis. *Biophys. J.* **92,** 1792–1805 (2007).

44. Fleming, R. M. T., Thiele, I. & Nasheuer, H. P. Quantitative assignment of reaction directionality in constraint-based models of metabolism: application to Escherichia coli. *Biophys. Chem.* **145,** 47–56 (2009).

45. Bennett, B. D. *et al.* Absolute metabolite concentrations and implied enzyme active site occupancy in Escherichia coli. *Nat. Chem. Biol.* **5,** 593–599 (2009).

46. Bordel, S. & Nielsen, J. Identification of flux control in metabolic networks using non-equilibrium thermodynamics. *Metab. Eng.* **12,** 369–377 (2010).

47. Noor, E. *et al.* Pathway Thermodynamics Highlights Kinetic Obstacles in Central Metabolism. *PLoS Comput. Biol.* **10,** e1003483 (2014).

48. Schrödinger, E. *What Is Life? The Physical Aspect of the Living Cell*. (Cambridge University Press, 1944).

49. Okabe, K. *et al.* Intracellular temperature mapping with a fluorescent polymeric thermometer and fluorescence lifetime imaging microscopy. *Nat. Commun.* **3,** 705 (2012).

50. Lane, N. Hot mitochondria? *PLOS Biol.* **16,** e2005113 (2018).

51. Baffou, G., Rigneault, H., Marguet, D. & Jullien, L. A critique of methods for temperature imaging in single cells. *Nat. Methods* **11,** 899–901 (2014).

52. Weber, J. K., Shukla, D. & Pande, V. S. Heat dissipation guides activation in signaling proteins. *Proc. Natl. Acad. Sci.* **112,** 10377–10382 (2015).

505   53.   Slochower, D. R. & Gilson, M. K. Motor-Like Properties of Non-Motor Enzymes. *bioRxiv* 121848
506   (2018). doi:10.1101/121848

507   54.   Riedel, C. *et al.* The heat released during catalytic turnover enhances the diffusion of an enzyme.
508   *Nature* **517,** 227–230 (2014).

509   55.   Golestanian, R. Anomalous diffusion of symmetric and asymmetric active colloids. *Phys. Rev.*
510   *Lett.* **102,** 188305 (2009).

511   56.   Gallet, F., Arcizet, D., Bohec, P. & Richert, A. Power spectrum of out-of-equilibrium forces in
512   living cells: amplitude and frequency dependence. *Soft Matter* **5,** 2947 (2009).

513   57.   Milstein, J. N., Chu, M., Raghunathan, K. & Meiners, J. C. Two-color DNA nanoprobe of
514   intracellular dynamics. *Nano Lett.* **12,** 2515–2519 (2012).

515   58.   Weber, S. C., Spakowitz, A. J. & Theriot, J. A. Nonthermal ATP-dependent fluctuations
516   contribute to the in vivo motion of chromosomal loci. *Proc. Natl. Acad. Sci.* **109,** 7338–7343
517   (2012).

518   59.   Chen, Y.-F., Milstein, J. N. & Meiners, J.-C. Protein-mediated DNA loop formation and
519   breakdown in a fluctuating environment. *Phys. Rev. Lett.* **104,** 258103 (2010).

520   60.   Milstein, J. N. & Meiners, J.-C. On the role of DNA biomechanics in the regulation of gene
521   expression. *J. R. Soc. Interface* **8,** 1673–81 (2011).

522   61.   Kochanowski, K. *et al.* Functioning of a metabolic flux sensor in Escherichia coli. *Proc. Natl.*
523   *Acad. Sci.* **110,** 1130–1135 (2013).

524   62.   Nilsson, A., Nielsen, J. & Palsson, B. O. Metabolic Models of Protein Allocation Call for the
525   Kinetome. *Cell Syst.* **5,** 538–541 (2017).

526   63.   Burgard, A. P., Nikolaev, E. V, Schilling, C. H. & Maranas, C. D. Flux coupling analysis of
527   genome-scale metabolic network reconstructions. *Genome Res.* **14,** 301–12 (2004).

528   64.   Drud, A. S. CONOPT—A Large-Scale GRG Code. *ORSA J. Comput.* **6,** 207–216 (1994).

529   65.   Hastie, T. J. ., Tibshirani, R. & Friedman, J. The elements of statistical learning: data mining,

530   inference, and prediction. (2011).

531   66.   Schellenberger, J., Lewis, N. E. & Palsson, B. Ø. Elimination of Thermodynamically Infeasible

532   Loops in Steady-State Metabolic Models. *Biophys. J.* **100,** 544–553 (2011).

533

534

535 **Figure 1. Overview of the workflow and model used.** We developed combined thermodynamic and stoichiometric constrained-
536 based models for *Saccharomyces cerevisiae* and *Escherichia coli*. With these models and experimental data, we performed
537 regression analyses to identify model parameters, amongst which is the limiting rate of cellular Gibbs energy dissipation. Using
538 these parameters in flux balance analyses, we then predicted various cellular phenotypes. S is the stoichiometric matrix, v the
539 rates of the respective processes (i.e. fluxes), c the metabolite concentrations, $\Delta_r G$ the Gibbs energies of reaction, $\Delta_f G$ the
540 metabolites' Gibbs formation energies, g the Gibbs energy dissipation rates, and the subscript *MET* denotes metabolic processes
541 and *EXG* exchange processes with the environment. Detailed model descriptions can be found in the Supplementary Methods
542 1.1-1.6, with the *S. cerevisiae*-specific details in Supplementary Note 1 and the *E. coli*-specific details in Supplementary Note 2.
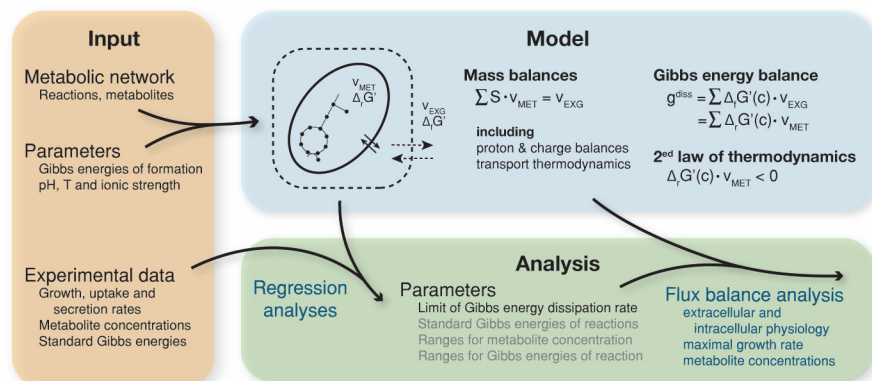

543

544   **Figure 2. Rate of cellular Gibbs energy dissipation does not exceed an upper limit.** The median Gibbs energy dissipation
545   rate, g^{diss} (black dots), as determined by regression analysis including a parametric bootstrap (n = 2000) using the combined
546   thermodynamic and stoichiometric constrained-based model, the physiological and metabolome data[17] and the Gibbs energies
547   from the component contribution method[18], reached an upper limit, which coincides with the onset of aerobic fermentation, i.e.
548   ethanol excretion. g^{diss}_{lim} was determined from the g^{diss} values at the plateau. The solid red line represents the median of those
549   values and the dashed red lines the 97.5% confidence interval. Note that although the regression was largely underdetermined
550   (107 degrees of freedom, Supplementary Fig. 2a), g^{diss} could be estimated with high confidence, because g^{diss} could in principle
551   already directly be estimated using perfect physiological rate measurements (compare SEq. 4 in Supplementary Method 1.2).
552   Error bars represent the 97.5% confidence intervals as determined by the parametric bootstrap (n = 2000).
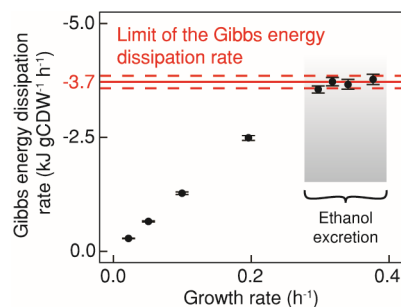

553

554   **Figure 3. Accurate predictions of cellular physiology with flux balance analysis (FBA) using the combined**
555   **thermodynamic and stoichiometric model constrained by g^{diss}_{lim}. (a–d)** Predictions of physiological rates for *S. cerevisiae*
556   growth on glucose (solid black line) with growth maximization as objective and constrained by the identified upper limit in the
557   Gibbs energy dissipation rate, g^{diss}_{lim}, of -3.7 kJ gCDW^{-1} h^{-1} as a constraint. Red circles represent experimentally determined
558   values from glucose-limited chemostat cultures[17,23] and red triangles values from glucose batch cultures[23,24]. The black arrow
559   points to the GUR at which the maximum growth rate was observed; solid grey lines represent predictions above this GUR.
560   Notably, at GURs >22 mmol gCDW^{-1} h^{-1} we found that the growth rate decreased again and cells started to massively increase
561   glycerol production. The fact that we could not find any experimental values with GURs >22 mmol gCDW^{-1} h^{-1} suggests that
562   cells restrict their glucose uptake rate in order to retain the maximal possible growth rate. The dotted black lines represent FBA
563   simulations with growth maximization as an objective, but without a constraint in g^{diss}. The dashed black lines represent
564   predictions with the 'minimal sum of absolute fluxes' as an objective and the g^{diss}_{lim}-constraint. The excellent predictions are not
565   a trivial result of our earlier regression as shown through sensitivity analyses with regards to various model parameters, e.g. lower
566   and upper bounds of intracellular metabolite concentrations, and the Gibbs energies of reaction (Supplementary Fig. 3-5).
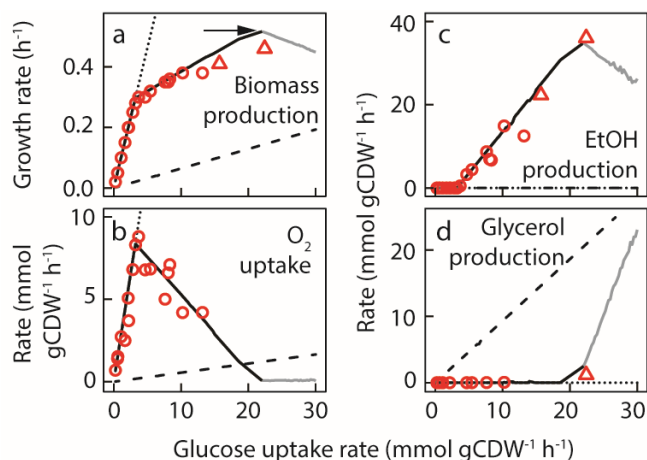
567

568   **Figure 4. Accurate predictions of intracellular fluxes with flux balance analysis (FBA) using the model constrained by**
569   g^{diss}_{lim}. **(a–d)** FBA predicted and through ^{13}C based metabolic flux analysis inferred intracellular fluxes at key branch points in
570   the central metabolism. These FBA predictions were obtained by means of flux variability analysis with the growth rates fixed to
571   the values obtained in the FBA optimizations and sampling of the solution space (Supplementary Fig. 8 and Supplementary
572   Methods 2.3 and 2.4). The graphs show flux boundaries from flux variability analyses (light grey areas) and the multivariate
573   distribution of intracellular fluxes obtained by sampling the solution space (n = 10'000'000) of the g^{diss}_{lim}-constrained model for
574   optimal growth rates, with the black lines representing medians and the dark blue areas the 97.5% confidence intervals. The
575   symbols denote fluxes determined by ^{13}C-based metabolic flux analysis; diamonds data[25]; squares[26]; triangles[27]; circles[28]. Note
576   that the models used for these ^{13}C-based metabolic flux analyses were small networks with about 20-30 reactions and included
577   heuristic assumptions on the reversibility of metabolic reactions. Therefore, these flux estimates may contain errors and biases as
578   discussed in Ref. [25] and should be understood as a comparison rather than a benchmark. PGI: glucose-6-phosphate isomerase;
579   GND: phosphogluconate dehydrogenase; PDHm: pyruvate dehydrogenase; SUCOAS1m: succinate-CoA ligase. Additional
580   intracellular fluxes are shown in Supplementary Fig. 7.
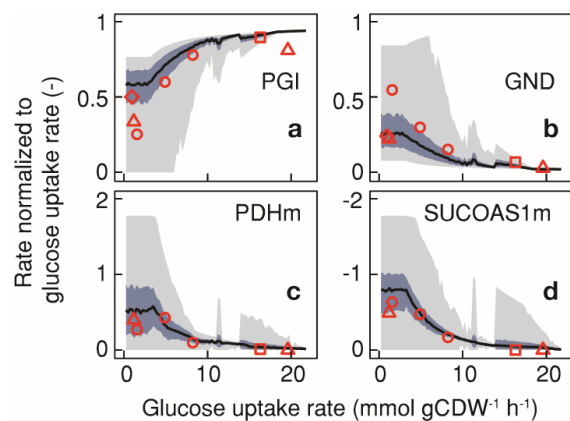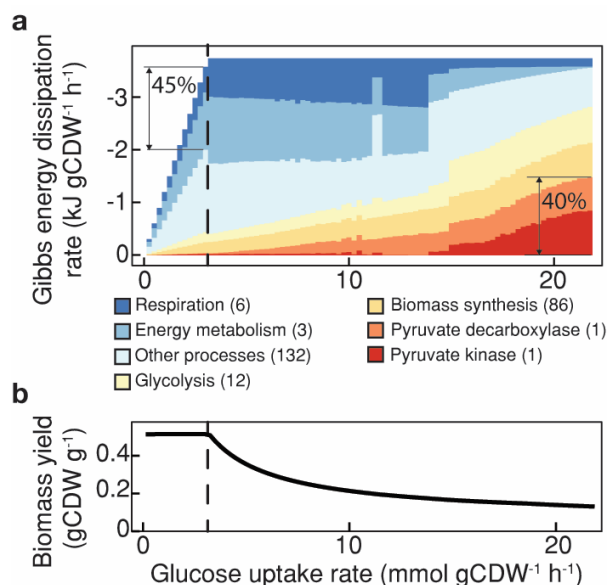

581

582   **Figure 5. Predictive capabilities of flux balance analysis (FBA) using the genome-scale combined thermodynamic and**
583   **stoichiometric model of *E. coli* constrained by g^{diss}_{lim}. (a)** Predictions of physiological rates for *E. coli* growth on glucose with
584   growth maximization as objective and the identified upper limit in the Gibbs energy dissipation rate, g^{diss}_{lim}, of -4.9 kJ gCDW^{-1} h^{-}
585   ^{1} as a constraint (solid black line). Red circles represent experimentally determined values from glucose-limited chemostat
586   cultures[30,32–35], and red triangles values from glucose batch cultures[36]. The black arrow points to the GUR, at which the maximum
587   growth rate was obtained in the simulation; solid grey lines represent predictions above this GUR and the shaded grey area the
588   variability determined through variability analysis. **(b)** Predictions of the maximal growth phenotype for growth on eight
589   different carbon sources, on simultaneously present glucose and succinate, or on either glucose or glycerol supplemented with all
590   proteinogenic amino acids; in all cases allowing for unlimited carbon source uptake[37–39]. The horizontal error bars represent the
591   variability determined at the optimal solution. The goodness of FBA predictions was assessed using the person correlation
592   coefficient (*r*), where the p-values were derived using Student's *t*-test. **(c)** Concentration profiles of three metabolites (coenzyme
593   A (CoA), ribose-5-phosphate (r5p) and α-ketoglutarate (akg)), which in our simulations showed a correlative behavior with GUR,
594   and for which experimental data were available. The experimental metabolite profiles were obtained in accelerostat experiments
595   with MG1655[33]. Note that here the onset of acetate production occurs at a lower GUR of 3.6 mmol gCDW^{-1} h^{-1}. For both, the
596   predictions and experimental data, the concentration profiles (solid grey line) were obtained using a local polynomial regression
597   method.
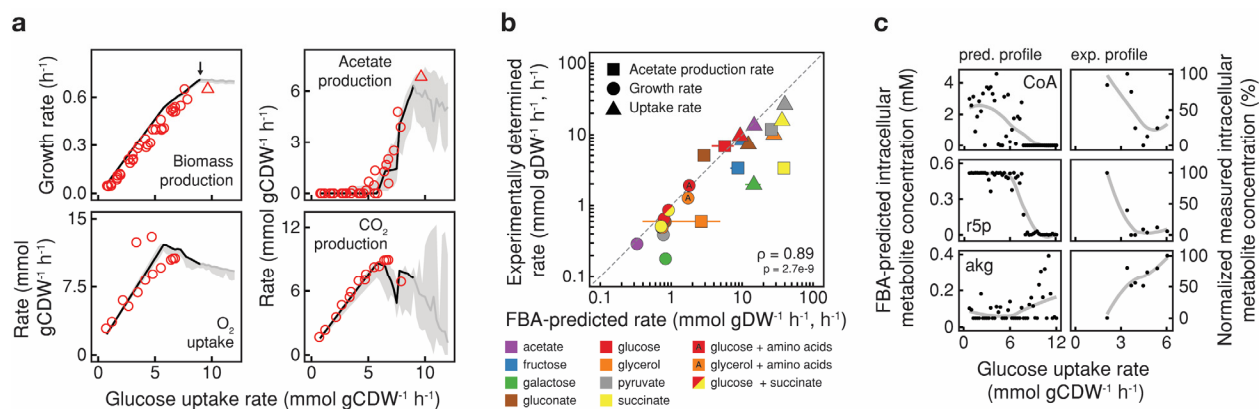
598

599 **Figure 6. Cells redistribute flux to avoid critical Gibbs energy dissipation rates. (a)** The limit in the Gibbs energy dissipation
600 rate causes flux redistribution with increasing GURs, globally leading to a change from respiratory to fermentative pathways.
601 Seven clusters of metabolic processes were identified by cluster analysis using the Euclidean distance between the Gibbs energy
602 dissipation rates of metabolic processes at different GURs (for details of the processes in the clusters refer to Supplementary Fig.
603 15). The Gibbs energy dissipation rates of the metabolic processes were obtained by sampling the solution space of the g^{diss}_{lim}-
604 constrained model for optimal growth. The numbers in brackets indicate the number of processes in each cluster. The dashed line
605 indicates the GUR at which ethanol production starts. An identical analysis of the data from the regression yielded similar results
606 (compare Supplementary Fig. 16). Out of the 31 possible ATP or NAD(P)H consuming futile cycles, none carried a flux in the
607 FBA optimizations and thus Gibbs energy is not dissipated through futile cycles. **(b)** The shift to less carbon-efficient pathways
608 leads to reduced biomass yields with increasing GURs.

609

26